ISBN: 978-3-95450-231-8 ISSN: 2673-5490 doi: 10.18429/JACoW-IPAC2023-MOPA100

PROTECTION OF EXTRACTION SEPTA DURING ASYNCHRONOUS BEAM DUMPS IN HL-LHC OPERATION

E. Farina*, M. Atanasov, J. Borburgh, C. Bracco, Y. Dutheil, A. Lechner, J. Maestre, P. Andreu Muñoz, F.X. Nuiry, P. Schwarz, C. Sharp, P. A. Thonet, R. Franqueira Ximenes
CERN, Geneva, Switzerland

Abstract

The LHC beam dump system was developed to safely and reliably dispose of the LHC beams at the end of physics fills or in case of emergency aborts. The beams are extracted by means of kicker magnets, deflecting the beams horizontally, and septa, which provide a vertical kick. The system must be able to cope with rare failure scenarios, such as an asynchronous beam dump, where the rise time of the extraction kickers is not synchronized with the 3 µs long particle-free abort gap. This type of event would lead to bunches impacting on downstream accelerator equipment if not properly absorbed by a system of beam-intercepting devices. In the High Luminosity-LHC (HL-LHC) era, the protection absorbers have to withstand significantly higher bunch intensities of up to $2.3 \cdot 10^{11}$ protons. In this paper, we study the robustness and protection efficiency of the septum protection absorbers for HL-LHC operation. In particular, we present energy deposition simulations for the absorber blocks and downstream equipment and define the required absorber upgrades for HL-LHC.

INTRODUCTION

The LHC beam dump system is composed of 15 fast-pulsed kicker magnets and 15 Lambertson septa (MSDs), which deflect the beam into the dump channel by applying horizontal and vertical kicks, respectively [1]. A series of dilution kickers in the extraction line sweep the beam across the dump front face, hence diluting the energy deposited by different bunches in the transverse planes [1]. To account for the rise time of the extraction kickers, the bunch filling scheme contains a 3 µs-long region of empty buckets, called abort gap. During regular beam dumps, the kickers are fired synchronously with the abort gap and all the bunches experience the same kick amplitude. A loss of synchronization can, however, occur in case of timing errors or the erratic pre-firing of an extraction kicker. In these events, a fraction of the circulating bunches can experience a partial deflection, being swept across the machine aperture [2].

To avoid damaging the downstream machine equipment, different beam absorbers are installed in the extraction region, which intercept mis-steered bunches during extraction system failures. One of these absorbers, called TCDS (Target Collimator Dump Septum), is placed upstream of the septa and protects the septum blade, as well as the vacuum chambers of the circulating beam and the extraction line. The TCDS was originally designed to sustain the impact of 7 TeV bunches with a bunch intensity of $1.7{\cdot}10^{11}$ protons [3]. In the High-Luminosity (HL) LHC era, starting in LHC Run 4 (from 2029), the bunch intensity will increase to $2.3{\cdot}10^{11}$ protons [4]. This requires a new assessment of the material robustness of TCDS blocks for accidental beam loss scenarios, considering the significantly higher energy deposition density induced by the HL-LHC beams. In addition, the protection efficiency of the TCDS has to be reassessed. In this paper, we present energy simulation studies for the absorber blocks, as well as the downstream septa. Finally, we discuss the required upgrades for HL-LHC operation.

ABSORBER BLOCK ROBUSTNESS

The TCDS diluter consists of two 3.3 m-long vacuum tanks, with 250 mm-long interconnecting bellows. In each of the two tanks, the actual intercepting device consists of two rows of diluter blocks. The first one aims at protecting the region between the vacuum chamber of the circulating beam and the extraction line of the downstream septa. The second extends the protection after the extraction line, for higher-than-nominal kick angles. The internal structure of each of the two 3-meter-long absorbing devices (TCDSU and TCDSD, upstream and downstream respectively) is composed of a series of isostatic graphite and Carbon-Fiber-Reinforced-Carbon (CfC) blocks. The final two TCDSD blocks are made of titanium alloy (Ti-6Al-4V, grade 5) [5]. Moreover, the size, positioning and orientation of the TCDS diluter blocks have been optimized to maximize the protection of the MSD magnets. In particular, the blocks are slightly tilted and have increasing thickness to account for the increasing separation between the circulating and extracted beams [2]. Figure 1 shows a simplified schema of the TCDS absorbing blocks: for each jaw the length, material and block density is reported. The lower material density is adopted at the shower maximum, to limit the energy deposition and temperature increase.

In case of an erratic pre-firing of an extraction kicker, all the other kickers are almost immediately triggered (within 1.3 µs), without any synchronization with the RF, leading to up to 48 bunches being swept across the TCDS. The local energy density deposited in the TCDS depends on the sweep velocity, which determines the bunch density impacting the absorbers. In particular, the bunch density is minimum in the region of the TCDS closer to the vacuum chamber of the circulating beam, and increases by moving towards the extraction line. In total, about 1.7% of the total beam energy may be deposited in the TCDS. In case of HL-LHC, this is equivalent to about 12 MJ [6]. In view of HL-LHC, not only

* edoardo.maria.farina@cern.ch

ISBN: 978-3-95450-231-8 ISSN: 2673-5490 doi: 10.18429/JACoW-IPAC2023-MOPA100

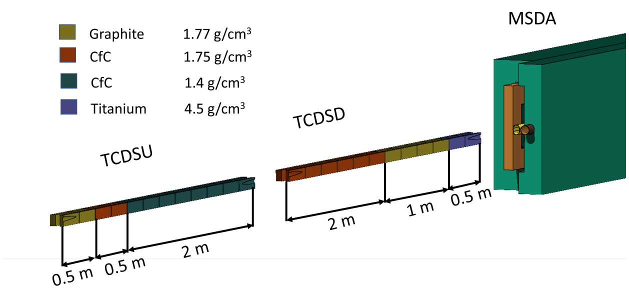

Figure 1: Simplified view of the TCDSU and TCDSD absorbing devices: the block material and density is also reported.

the effectiveness of the device in protecting the downstream magnets, but also its own survival needs to be assessed in the worst accidental case foreseen. To address the device robustness, FLUKA [7–9] simulations have been carried out to compute the energy deposition in each graphitic and titanium block. In Fig. 2 the simulated peak energy density in the internal row of TCDS blocks for a bunch intensity of $2.3 \cdot 10^{11}$ protons per bunch is shown. Different colors highlight different materials: the maximum peak is reached in the first vacuum tank, at about 2 m from the TCDS front face.

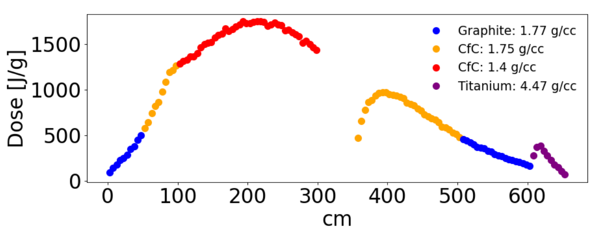

Figure 2: Energy density deposited in the TCDS blocks following an erratic with HL-LHC beams.

In particular the following energy densities are scored:

- 1800 J/g in the low-density CfC absorber blocks.
- 1300 J/g and 900 J/g in the isostatic graphite in the first and second vacuum tank, respectively.
- 450 J/g in the Titanium blocks (730 °C).

Dynamic thermo-structural finite element studies were performed for the most highly loaded blocks using ANSYS® Workbench™ and LS-DYNA®. With the volumetric distribution of energy deposition calculated in FLUKA applied to the finite element model, the short-timescale dynamic thermo-structural response was simulated, capturing peak temperatures, shockwaves and vibration behaviour. In the case of graphite, results of explicit simulations were post-processed based on the Christensen failure criteria for brittle materials. Utilisation factors exceeding a value of one indicated the expected structural failure of these blocks under the specified HL-LHC conditions. It is therefore necessary to replace the graphite with a non-fragile and more robust material solution (CfC) prior to HL-LHC operation. Meanwhile, implicit simulations of the titanium alloy blocks indicated plastic deformation caused by the thermal stresses and dynamic response to beam impact. Whilst not ideal, this could be considered acceptable for one high intensity asynchronous dump event; the expected robustness, when subjected to multiple events, is currently under review. For the currently installed CfC blocks, which absorb the majority of the energy, the simulation is affected by a large uncertainty. The robustness of these blocks was therefore tested in the CERN HiRadMat facility, where, when exposed up to 2.7 kJ/g, the material showed no observable damage [10]. To conclude, whilst engineering studies on the TCDS are ongoing, further upgrade beyond the replacement of the graphite blocks is not foreseen.

ENERGY DEPOSITION IN THE SEPTA

Downstream of the TCDS, 15 MSD septum magnets are installed. They are of three different types, MSDA, MSDB, MSDC. The yokes are composed of two half cores, coil and septum core, respectively. The septum core hosts the vacuum chamber for the circulating beam. The three septa types differ in their septum thickness, number of coil layers and distance of the circulating beam from the pole [11]. A transversal view of the MSDA septum, as implemented in FLUKA, is given in Fig. 3 (a), where the yokes (green), the coils (bronze) and the vacuum chambers are shown. The projection of the TCDS rows on the front of the first MSDA is also shown. The calculated magnetic field map has then been applied to the geometry for each of the three MSD septa configurations. In order to validate its implementation, the trajectory of a proton tracked by FLUKA has been compared to the LHC expected beam position. Figure 4 shows the achieved agreement in the vertical position (within a few µm) confirming the good description of the magnetic field.

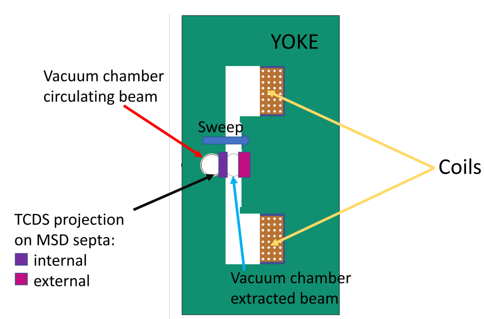

Figure 3: FLUKA model of the MSDA septum; the projection of the TCDS blocks on the front face of the septum is also shown.

Figure 5 shows the model of the first MSDA, with the superimposed energy deposition as calculated by FLUKA simulations. The TCDS (not shown) is installed just before the element in the figure. As suggested by the color code, the highest energy deposition in the yokes occurs at the internal side of the vacuum chamber of the circulating beam, where

ISBN: 978-3-95450-231-8 ISSN: 2673-5490 doi: 10.18429/JACoW-IPAC2023-MOPA100

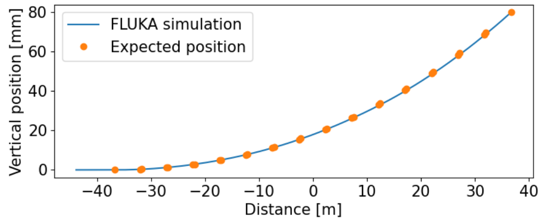

Figure 4: Trajectory study: simulated beam trajectory in magnetic field is compared with expected trajectory.

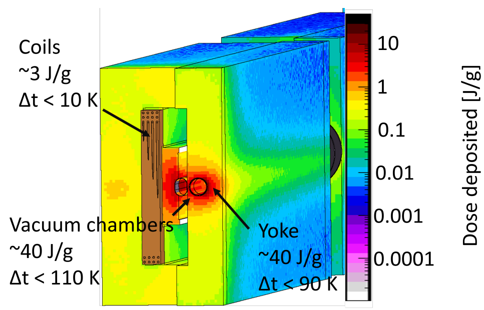

Figure 5: FLUKA model of the first MSDA superimposed with the energy deposited. The highest energy density is scored in the septum core, at the side of the circulating beam vacuum chamber. The adiabatic temperature increase is also reported.

the TCDS shadow projection is minimal. Figure 6 shows the maximum energy deposition, which is scored in the yokes, as a function of the distance from the TCDS, for the 15 septa. Different colors help to distinguish among the three different magnet types. The maximum value, scored in the region closer to the TCDS is of about 40 J/g, which corresponds to an adiabatic temperature increase of 110 °C, considering a density of 7.87 g/cm^3 and a specific heat of 0.5 J/(g·K). Furthermore, it should be noticed that no additional hot-spots are observed in the downstream septa. This temperature is not critical concerning a possible change in the magnetic properties of the lamination (up to 150 °C is considered as acceptable). Moreover, problems in the coils are expected in the event of continuous operation at more than 60 °C, while this accidental case is characterized by an instantaneous (µs) heating process.

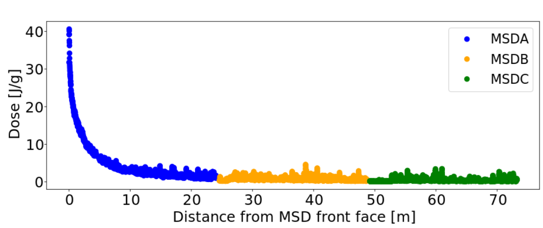

Figure 6: Maximum energy density scored in the yokes as a function of the distance from the TCDS. Different colors highlight the different septa types.

In addition to the yokes, dedicated studies have been performed addressing the two vacuum chambers for the circulating and extracted beam, respectively. The circulating beam vacuum chamber is made of copper, surrounded by a mu-metal (nickel–iron soft ferromagnetic alloy) coating. The extracted beam vacuum chamber, on the other hand, is made of stainless steel. Figure 7 shows the maximum energy density deposited in the vacuum chambers, in the copper (a), in the mu-metal (b) and in the stainless-steel (c), as a function of the distance from the TCDS. The final maximum adiabatic temperature increase is estimated at 110 °C in the copper, 95 °C in the mu-metal and 60 °C in the stainless steel. In all cases results are well below the 300 °C limit [1]. To conclude, an erratic pre-firing of an extraction magnet in HL-LHC has been estimated to lead, with the current design of the TCDS, to energy deposition and temperature increases that are within acceptable limits of operation of the device.

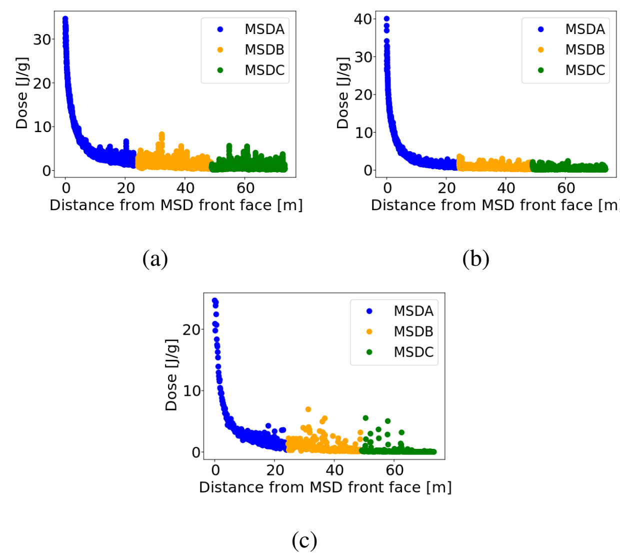

Figure 7: Maximum energy density scored in the copper circulating beam vacuum chamber (a), in the Mu-metal circulating beam vacuum chamber (b) and in the aluminium extracted beam vacuum chamber (c).

CONCLUSIONS

FLUKA and thermo-mechanical simulation studies have been carried out to assess the need of upgrading the septum protection device to cope with the increase of beam intensity expected in HL-LHC, in case of an erratic pre-firing of kicker magnets. Concerning the TCDS, isostatic graphite needs to be replaced with CfC of similar density in order to guarantee the absorbers robustness during operation. Concerning the MSD septa, temperature increase and energy deposited have been estimated to remain within acceptable limits in case of an erratic, thus not requiring any further upgrade of the upstream dilution blocks.

ISBN: 978-3-95450-231-8 ISSN: 2673-5490 doi: 10.18429/JACoW-IPAC2023-MOPA100

REFERENCES

[1] W. Weterings *et al.*, "TCDS diluter to protect MSD septum magnets", CERN, Geneva, Switzerland, Functional specification LHC-TCDS-ES-0001, Jun. 2003.

[2] B. Goddard and M. Gyr, "The Aperture and Layout of the LHC Extraction Septa and TCDS Diluter with an Enlarged MSDC Vacuum Chamber", CERN, Geneva, Switzerland, LHC project note 320, Aug. 2003.

[3] W. Weterings *et al.*, "Conceptual Design of the LHC Beam Dumping Protection Elements TCDS and TCDQ", CERN, Geneva, Switzerland, LHC-Project-Report-756, 2004.

[4] I. Béjar Alonso *et al.*, "High-Luminosity Large Hadron Collider (HL-LHC): Technical Design Report", CERN, Geneva, Switzerland, 2020. doi:10.23731/CYRM-2020-0010

[5] T. Kramer, "LHC Beam Dump System: Analysis of beam commissioning, performance and the consequences of abnormal operation", CERN-THESIS-2011-135, Ph.D. thesis, Graz, Tech. U., 2011.

[6] C. Bracco *et al.*, "LBDS Performance in RUN 2", in *Proc. 9th LHC Operations Evian Workshop*, Evian Les Bains, France, 2019, pp. 131–134.

[7] C. Ahdida *et al.*, "New Capabilities of the FLUKA Multi-Purpose Code", *Front. Phys.*, vol. 9, p. 788253, 2022. doi:10.3389/fphy.2021.788253

[8] G. Battistoni *et al.*, "Overview of the FLUKA code", *Ann. Nucl. Energy*, vol. 82, pp. 10–18, 2015. doi:10.1016/j.anucene.2014.11.007

[9] V. Vlachoudis, "FLAIR: A Powerful But User Friendly Graphical Interface For FLUKA", in *Proc. Int. Conf. on Mathematics, Computational Methods & Reactor Physics 2009*, Saratoga Springs, New York, 2009, pp. 790–800.

[10] P. Andreu Muñoz *et al.*, "Irradiation of Low-Z Carbon-Based Materials with 440 GeV/c Proton Beam for High Energy & Intensity Beam Absorbers: The CERN HiRadMat-56-HED Experiment", in *Proc. IPAC'22*, Bangkok, Thailand, Jun. 2022, pp. 2883–2886. doi:10.18429/JACoW-IPAC2022-THPOTK049

[11] M. Sassowsky *et al.*, "Steel Septum Magnets for the LHC Beam Injection and Extraction", in *Proc. EPAC'02*, Paris, France, Jun. 2002, paper MOPLE083, pp. 2514–2516.